




Electron dynamics in fused silica after strong field laser excitation detected by spectroscopic imaging pump-probe ellipsometry

Theo Pflug ,* Markus Olbrich , and Alexander Horn 

Hochschule Mittweida, Laserinstitut Hochschule Mittweida, Technikumplatz 17, 09648 Mittweida, Germany



(Received 17 February 2022; revised 30 June 2022; accepted 30 June 2022; published 14 July 2022)

Laser ablation of dielectrics by ultrashort pulsed laser radiation is induced by nonlinear photoexcitation, such as multiphoton and tunneling processes, and the subsequent impact excitation, due to electron-electron collisions. Previous theoretical and experimental studies demonstrate that these two phenomena strongly depend on the transient optical properties of the dielectric and the electron-electron collision times. To estimate these transient optical properties and the collision time, the excited electrons are usually considered as a nearly free-electron gas, being described by the Drude theory. All previous experimental studies support using the Drude theory by time-resolved measurements of the transient reflectance during and after irradiation. However, a comprehensive characterization of the transient complex refractive index, and, thus, a more complex view of the optical properties upon irradiation above the ablation threshold fluence was still missing. Therefore, this paper presents the time-, spectral-, and fluence-resolved complex refractive index of fused silica during the interaction with ultrashort pulsed laser radiation (800 nm, 40 fs, and 4.4 J/cm²) measured by spectroscopic imaging pump-probe ellipsometry. Comparing the state-of-the-art Drude model to the experimental data reveals that, although the Drude model replicates the transient reflectance of the material, it deviates significantly from the transient refractive index in the considered temporal range up to 200 fs after irradiation. Thus, the Drude model cannot correctly describe the transient optical properties, which leads to the assumption that the electrons cannot be considered as a nearly free-electron gas at this time. Alternatively, a Lorentz model, considering the excited electrons as bound, can replicate the measured data much better, which indicates that the electrons might be excited into localized states.

DOI: [10.1103/PhysRevB.106.014307](https://doi.org/10.1103/PhysRevB.106.014307)

I. INTRODUCTION

Nonlinear photoexcitation of atoms and molecules due to ultrashort pulsed laser irradiation at high intensities enables the generation of microstructures inside dielectric bulk materials. Therefore, numerous new structuring procedures emerged over the past few decades, such as the scribing of microfluid channels for “lab-on-a-chip” devices [1–3], the generation of biologic degradable stents or osteosynthesis components [4], the so-called stealth dicing method [5,6], cutting the flap for laser eye surgery [7], and the highly precise microstructuring of organic materials being utilized in photovoltaics [8,9]. Contrary to linear photoexcitation, nonlinear processes enable to excite electrons from the valence-band (VB) into the conduction band of a material, even though the band-gap energy of the material exceeds the photon energy of the incident laser radiation. In literature, multiphoton and tunnel excitations are assumed to represent the driving mechanisms for nonlinear excitation, both becoming probable at intensities of a few TW/cm² [10–12]. These processes are referred to as nonlinear because the kinetic energy of the excited electrons is not directly proportional to the photon energy, and the number of

excited electrons is not directly proportional to the intensity of the laser radiation.

Electrons excited by nonlinear photoexcitation can gain even more energy by transient intraband transitions due to contemporaneous acceleration by the oscillating electric laser field and collisions with third partners, which is often referred to as free carrier absorption or inverse bremsstrahlung [13–22]. When the energy difference to the lower edge of the conduction band of such an additionally excited electron exceeds the band-gap energy, electron-electron collisions become probable which can excite another electron into the conduction band by impact excitation [12,14]. This leads to a rapidly increasing electron density in the conduction band because electron-electron collisions become more probable the more excited electrons exist, resulting in an excitation avalanche.

When the absorbed energy density and with it the induced number of electrons in the conduction band of a dielectric exceed critical values, the material gets ablated. The threshold for this irreversible damage is often referred to as laser-induced damage threshold [23–28] whereby the induced electron density reaches orders of magnitude of 10²⁷–10²⁸ m⁻³ [22,29–31], resulting in a strongly increasing transient reflectance and absorbance of the dielectric upon irradiation [14,19,24,32–47]. Irradiating the material at the damage threshold is also accompanied by the onset of measurable plasma emissions [17,23], which is why the transient

*Also at Technische Universität Chemnitz, Institut für Physik, Reichenhainer Straße 70, 09126 Chemnitz, Germany; pflug@hs-mittweida.de

optical properties of excited dielectrics are referred to as those of a plasma and are usually described by the Drude theory in the literature [13–17,32–40,48–56].

However, the transition of the material from the solid state to the plasma state is hard to describe theoretically and not completely understood yet [17,57]. Since previous experimental studies only applied pump-probe reflectometry to investigate the transient reflectance of dielectrics upon irradiation [14,19,24,33,34,36,37,40,43,50,54], no spectroscopic studies of the transient complex refractive index during irradiation at fluences near or above the damage threshold fluence exist to validate the assumed Drude-like behavior in a wide parameter range. In order to verify unambiguously whether the transient optical properties of fused silica (FS) are describable by the Drude theory during the transition from the solid state into the plasma state, this paper applies spectroscopic imaging pump-probe ellipsometry to investigate the transient complex refractive index of fused silica upon irradiation above the threshold fluence in a temporal range up to 200 fs after the excitation.

In the following, the optical properties of fused silica at rest and the transient optical properties (refractive index, extinction coefficient, and reflectance) of fused silica upon irradiation above the threshold fluence are presented. Then, two different dielectric function models are approximated to the measured data. The first model, namely, the state-of-the-art Drude model, considers the excited electrons as a nearly free-electron plasma [13–17,32–40,48–56]. The second model, referred to as Lorentz model, assumes that the excited electrons occupy localized bound states. This represents a new approach based on the assumption that the electrons are not nearly free directly after excitation. Instead, the excited electrons are still bound due to a strong interaction with the surrounding disordered ions of the amorphous fused silica [17,58], whereas the transition into a nearly free-electron plasma occurs afterwards [59]. An exact knowledge about the behavior of the excited electrons is necessary to estimate the linear excitation probability within the conduction band and, therefore, strongly affects the impact excitation rate in theoretical simulations [10,26].

II. MATERIAL AND METHODS

A. Optical properties of fused silica at rest

The investigated fused silica is UV grade fused silica (UV FS) provided by EKSMA Optics, UAB. The UV FS conforms the requirements for Shott glass SUPRASIL and is usually used for optical components. The amorphous dielectric fused silica (structural formula SiO_2) is an oxide of silicon with a tetrahedral structure with one silicon atom being bound to four oxygen atoms. Its molar mass and density are $M_m = 60.1$ g/mol and $\rho_{\text{rest}} = 2.2$ g/cm³, leading to a SiO_2 compound density of $n_a = 22.04 \times 10^{27}$ m⁻³. At room temperature, the valence-band of ideal fused silica is completely occupied, whereas the conduction band is empty with an electron density of $n_e = 0$. Thus, fused silica is transparent in the visible spectral range due to a band-gap energy of $E_{\text{gap}} \approx 9$ eV [14,48,63]. In this paper, the complex refractive index $\tilde{n} = n - ik$ of fused silica at rest is modeled by a single Lorentz oscillator [64]

representing the optical properties of the valence-band electrons by

$$\tilde{n}^2(\omega) = \varepsilon_\infty + \varepsilon_{\text{L,VB}} = \varepsilon_\infty + \frac{e^2}{\varepsilon_0 m_e} \frac{(n_a N_0 - n_e)}{\omega_0^2 - \omega^2 + i\Gamma_0 \omega}, \quad (1)$$

with the offset ε_∞ , the vacuum permittivity ε_0 , the electron rest mass m_e , the number of valence-band electrons per molecule N_0 , the electron density in the conduction-band $n_e = 0$, the resonance frequency ω_0 , the radiation frequency ω , as well as the damping constant Γ_0 . In order to derive the electron density $n_a N_0$, the resonance frequency ω_0 , and the damping constant Γ_0 , the Lorentz model is approximated to the complex refractive index \tilde{n} measured by a commercial and a self-constructed pump-probe ellipsometer, as well as to the refractive index n given in the literature (Fig. 1). See the Supplemental Material S.I for the explanation of the principle of ellipsometry and the corresponding data evaluation [62]. The resulting approximated parameters of the Lorentz model are $\varepsilon_\infty = 1.49$, $n_a N_0 = 44 \times 10^{27}$ m⁻³, $\hbar\omega_0 = 10$ eV, and $\hbar\Gamma_0 = 0.9$ eV. By considering the SiO_2 compound density of $n_a = 22.04 \times 10^{27}$ m⁻³, the number of the participating electrons per SiO_2 compound is determined to $N_0 = 1.996 \approx 2$. These are the starting parameters for the modeling of the transient dielectric function with the Lorentz term $\varepsilon_{\text{L,VB}}$ approaching zero with increasing electron density n_e in the conduction band. Although $\hbar\Gamma_0$ is larger than zero with this approximation, the resulting extinction coefficient is $k < 0.005$ in the visible spectral range and, thus, negligible.

B. Spectroscopic imaging pump-probe ellipsometry

An amplified Ti:sapphire laser system (Astrella, Coherent, Inc., $\lambda = 800$ nm, $\tau_H = 35$ fs, and $M^2 = 1.2$) provides ultrashort pulsed laser radiation, which is divided into pump and probe radiation by a beam splitter [65]. The wavelength of the probe radiation is changed in the range of 450 nm $\leq \lambda \leq 900$ nm using an optical parametric amplifier (TOPAS Prime, Light Conversion, Inc.). The pump radiation is focused onto the sample surface by a thin focusing lens ($f = 150$ mm) resulting in an applied peak fluence of $H_0 = 4.4$ J/cm² on the material surface. During the interaction of the pump radiation with the fused silica surface, the transient complex refractive index of the excited material is determined by pump-probe ellipsometry within the temporal range of -200 fs $\leq (t - t_0) \leq 200$ fs. At the temporal reference t_0 , the maximum of the temporal intensity distribution of the pump radiation interacts with the material surface. The temporal step width is set to $\Delta t = 40$ fs. The ellipsometer is based on the rotating compensator method and is combined with an imaging setup consisting of a microscope objective (20 \times , $N_A = 0.4$), a tube lens ($f = 200$ mm), and a CCD camera (GE 1024 1024 BI UV3, greateyes GmbH, 1024 \times 1024 pixel, pixel size 13 \times 13 μm^2). Because the focused pump radiation has a defined Gaussian fluence distribution $H(x, y) = H_0 \exp(-2\frac{x^2+y^2}{w_0^2})$ at the sample surface, the spatially resolved measurement enables to assign a local fluence $H(x, y)$ to each measured coordinate. See the Supplemental Material [62] for a detailed explanation of the experimental setup. The radiation source as well as the spectral and temporal properties of the

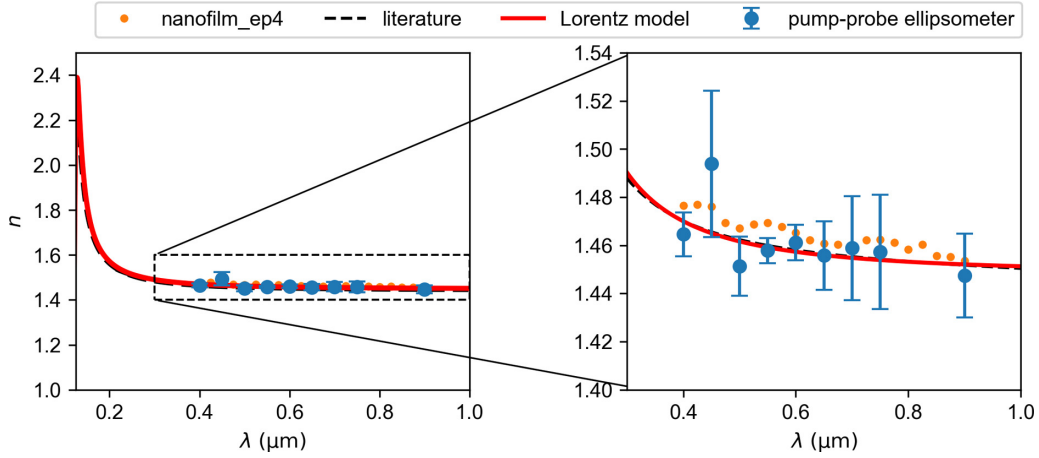


FIG. 1. Comparison of the refractive index n of fused silica given in the literature [60,61] (black), measured by a commercial ellipsometer (orange dots, nanofilm_ep4, Accurion GmbH), measured by the pump-probe ellipsometer [62] (blue dots), and approximated by a single Lorentz oscillator [red solid line, Eq. (1) with $\varepsilon_\infty = 1.49$, $n_a N_0 = 44 \times 10^{27} \text{ m}^{-3}$, $\hbar\omega_0 = 10 \text{ eV}$, and $\hbar\Gamma_0 = 0.9 \text{ eV}$] in a broad spectral range (left) and within the measurable range of the self-constructed and the commercial ellipsometer (right).

pump and probe radiation are discussed in Sec. S.II of the Supplemental Material [62]. The optical beam paths of pump and probe radiation, the evaluation of the measured data, and the determination of the temporal reference t_0 are explained in Supplemental Material S.III [62]. The ablation threshold of fused silica and the beam dimension w_0 of the applied pump radiation are determined in S.IV in the Supplemental Material [62].

III. RESULTS AND DISCUSSION

A. Transient optical properties

In order to investigate the electron excitation dynamics in fused silica upon irradiation with ultrashort pulsed laser radiation, spectroscopic imaging pump-probe ellipsometry is applied [65]. This method enables the comprehensive determination of the complex refractive index $\tilde{n} = n - ik$, consisting of the refractive index n and the extinction coefficient k , as a function of the probe wavelength λ , the temporal delay t between pump and probe radiation, and the local fluence $H(x)$ of the pump radiation. The applied pump radiation features a wavelength of $\lambda_{\text{pump}} = 800 \text{ nm}$, a pulse duration of $\tau_{H,\text{pump}} = 40 \text{ fs}$, and a peak fluence of $H_0 = 4.4 \text{ J/cm}^2$, which equals almost the twofold ablation threshold fluence $H_{\text{thr}} = (2.3 \pm 0.7) \text{ J/cm}^2$ of fused silica (see Supplemental Material S.IV [62]). The probe radiation has a pulse duration of $\tau_{H,\text{probe}} = 60 \text{ fs}$, an angle of incidence $\theta_0 = 60^\circ$, and its wavelength is varied in the spectral range of $450 \text{ nm} \leq \lambda \leq 900 \text{ nm}$ by an optical parametric amplifier (TOPAS Prime, Light Conversion, Inc.). The temporal delay between pump and probe radiation is varied in the range of $-200 \text{ fs} \leq (t - t_0) \leq 200 \text{ fs}$ with a step width of $\Delta t = 40 \text{ fs}$. To present the measured data in a clear and compact manner, the fluence and time-dependent refractive index $n(H(y=0, x), t, \lambda)$ and extinction coefficient $k(H(y=0, x), t, \lambda)$ are visualized as two-dimensional maps (Fig. 2). Additionally, the transient reflectance $R(H(y=0, x), t, \lambda)$ is calculated from the measured n and k by Fresnel's equations for a perpendicular angle of incidence [64] (Fig. 2 right). The whole measured data set of the

spatially, temporally, and spectroscopically resolved refractive index and extinction coefficient is reported in Supplemental Material S.V [62].

B. Transient dielectric function models

As described in the Introduction, the excited electrons in fused silica upon irradiation with ultrashort pulsed laser radiation are usually considered as a nearly free-electron plasma in the literature. The optical properties of such an electron plasma are described by the Drude theory, and, thus, the optical properties of the excited fused silica result then from the excited electrons (Drude term ε_D) as well as from the remaining bound electrons in the valence-band described by $\varepsilon_{L,\text{VB}}$ from Eq. (1) [64] both in dependence on the density of excited electrons n_e . The resulting transient dielectric function is given by

$$\begin{aligned} \tilde{n}_D^2(\omega) &= \varepsilon_\infty(n_e) + \varepsilon_{L,\text{VB}}(n_e) + \varepsilon_D(n_e) \\ &= \varepsilon_\infty(n_e) + \frac{e^2}{\varepsilon_0 m_e} \frac{(n_a N_0 - n_e)}{\omega_0^2 - \omega^2 + i\Gamma_0 \omega} \\ &\quad - \frac{e^2}{\varepsilon_0 m_e} \frac{n_e}{\omega^2 - i\omega/\tau_c} . \end{aligned} \quad (2)$$

The parameters of the Lorentz term $\varepsilon_{L,\text{VB}}$ are assumed to be constant and are directly taken from the determined Lorentz model of fused silica at rest (Sec. II A) with the electron density in the valence-band $n_a N_0 = 44 \times 10^{27} \text{ m}^{-3}$, the resonance energy $\hbar\omega_0 = 10 \text{ eV}$, and the damping energy $\hbar\Gamma_0 = 0.9 \text{ eV}$. With increasing density of the excited electrons n_e , the strength of the Lorentz term decreases, whereas the Drude term becomes dominant. The excited electron density n_e and the collision time τ_c of these electrons represent fit parameters, which are determined by approximating Eq. (2) to the measured optical properties from Fig. 2. The transient offset $\varepsilon_\infty(n_e)$ is calculated according to the Clausius-Mossotti (CM)

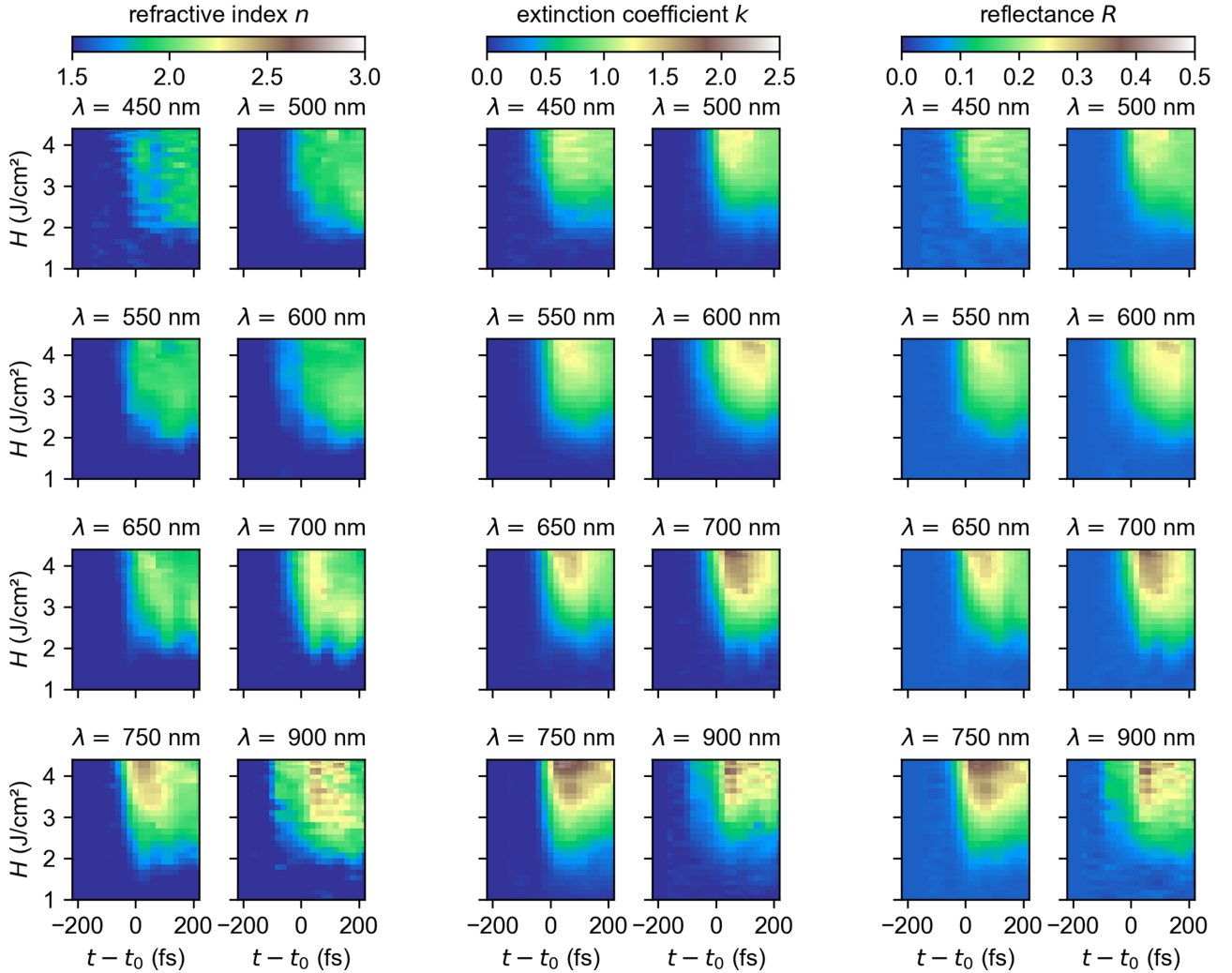


FIG. 2. Measured temporal evolution of the fluence-resolved refractive index $n(t, H)$, extinction coefficient $k(t, H)$, and reflectance $R(t, H)$ of fused silica at different probe wavelengths λ induced by single-pulsed pump irradiation at the peak fluence $H_0 = 4.4 \text{ J/cm}^2$.

correction [56,66],

$$\varepsilon_\infty(n_e) = 1 + \frac{3\beta_{\text{CM}}(n_a N_0 - n_e)/(n_a N_0)}{3 - \beta_{\text{CM}}(n_a N_0 - n_e)/(n_a N_0)}. \quad (3)$$

The Clausius-Mossotti parameter is determined to $\beta_{\text{CM}} = 0.421$ by considering the initial condition $\varepsilon_\infty(n_e = 0) = 1.49$ for fused silica at rest (Fig. 1). Although Eq. (2) represents a Lorentz-Drude model, it is simply referred to as the Drude model from now on.

Additionally to the state-of-the-art Drude model, a Lorentz-Lorentz model is used as an alternative to model the measured transient optical properties. The transient Lorentz-Lorentz model considers the excited electrons as bound in localized states similar to the valence-band electrons [58]. This new approach is based on the assumption that the excited electrons are not describable as a nearly free-electron gas in the temporal range up to 200 fs after excitation. Instead, the excited electrons still feature a strong Coulomb interaction with the surrounding disordered ions and the electron-phonon scattering only vanishes at later times [17]. The Lorentz-Lorentz model, thus, describes the valence-band electrons

($\varepsilon_{\text{L,VB}}$) as well as the excited electrons (ε_{L}), each using a Lorentz oscillator. The resulting transient dielectric function is then given by [64]

$$\begin{aligned} \tilde{n}_{\text{L}}^2(\omega) &= \varepsilon_\infty(n_e) + \varepsilon_{\text{L,VB}}(n_e) + \varepsilon_{\text{L}}(n_e) \\ &= \varepsilon_\infty(n_e) + \frac{e^2}{\varepsilon_0 m_e} \frac{(n_a N_0 - n_e)}{\omega_0^2 - \omega^2 + i\Gamma_0 \omega} \\ &\quad + \frac{e^2}{\varepsilon_0 m_e} \frac{n_e}{\omega_1^2 - \omega^2 + i\omega/\tau_c}, \end{aligned} \quad (4)$$

with ε_∞ from Eq. (3) and the same Lorentz parameters $n_a N_0$, ω_0 , and Γ_0 for fused silica at rest as applied in the Drude model. Analogous to the Drude model, the electron density n_e , and the collision time τ_c of the excited electrons represent fit parameters. Additionally, the resonance frequency ω_1 is also used as a fit parameter. Again, this Lorentz-Lorentz model is simply referred to as the Lorentz model in the further discussion.

For both models [Eqs. (2) and (4)], the transient electron density in the valence-band ($n_a N_0 - n_e$) must not become

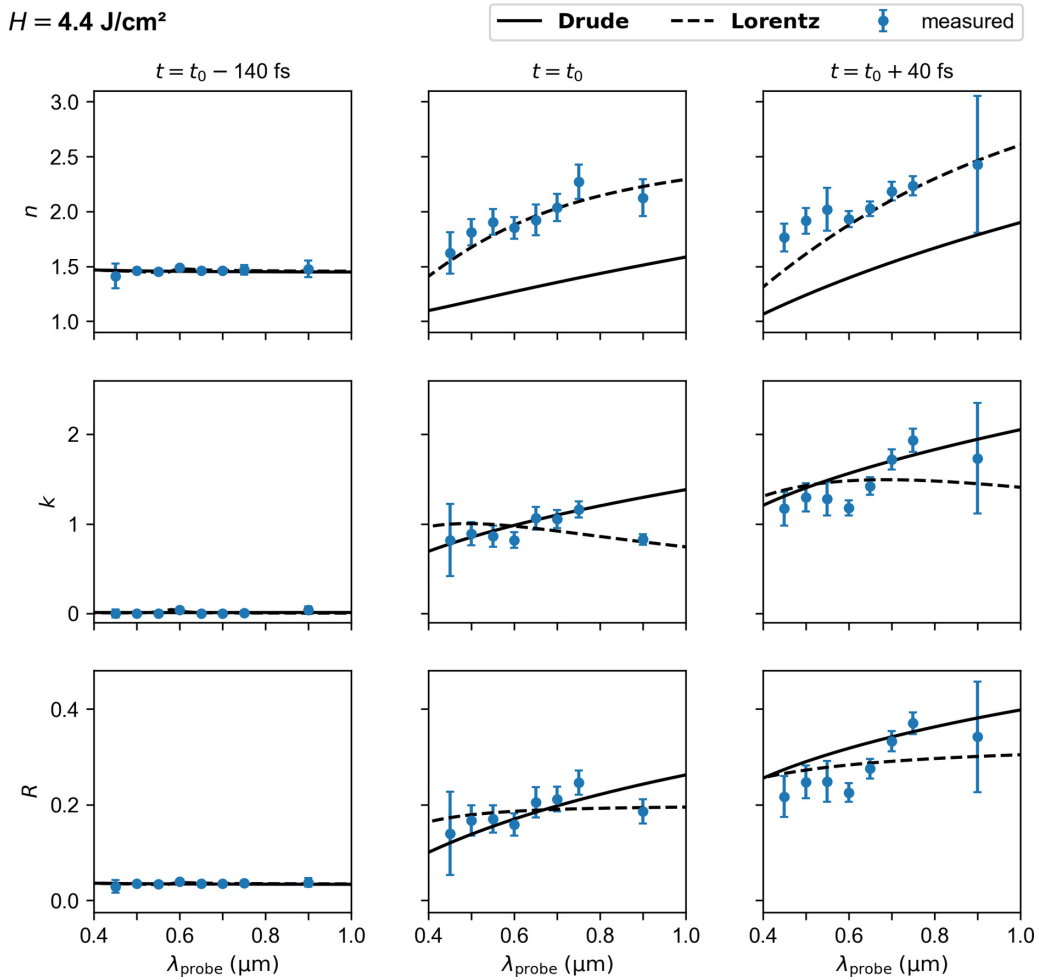


FIG. 3. Comparison of the measured refractive index n and extinction coefficient k , as well as the derived reflectance R for a normal angle of incidence of fused silica at different times t for the local fluence $H = 4.4 \text{ J/cm}^2$ of the exciting pump radiation with the approximated Drude [Eq. (2)] and Lorentz models [Eq. (4)] for the transient dielectric function.

negative for which reason the maximum inducible electron density in the conduction band for both approaches is constrained to $n_{e,\text{max}} = n_a N_0 = 44 \times 10^{27} \text{ m}^{-3}$. This maximum electron density is similar to the maximum conduction-band electron density determined in the literature, being in the range of $22 \times 10^{27} \text{ m}^{-3} < n_{e,\text{max}} < 100 \times 10^{27} \text{ m}^{-3}$ [14,34,36,53,63].

The Drude and the Lorentz models [Eqs. (2) and (4)] are fitted to the measured $n(H, t, \lambda)$ and $k(H, t, \lambda)$, as well as to the derived $R(H, t, \lambda)$ from Fig. 2 for each fluence and time step. In order to clearly compare the measured data with the fitted graphs, $n(\lambda)$, $k(\lambda)$, and $R(\lambda)$ are presented at the local fluence $H = 4.4 \text{ J/cm}^2$ for different exemplary times t first (Fig. 3). Before excitation at $t = t_0 - 140 \text{ fs}$, the optical properties of fused silica do not significantly differ from the values at rest. Therefore, both the Drude and the Lorentz model reproduce n , k , and R very well since no electrons occupy states in the conduction band with $n_e = 0$. However, for times $t \geq t_0$, the Drude model strongly differs from the measured n (Fig. 2 black solid lines), whereas k and R can be reproduced quite well. Contrary, the Lorentz model replicates all three transient optical properties in the considered temporal range (Fig. 2 black dashed lines).

In Fig. 3 the measured and fitted data are compared only for some exemplary times at one fluence in which the deviation between the measured optical properties and the models is only qualitatively ascertainable. To quantize this deviation, the sum of the normalized squared residuals D_{sq} between the measured and the fitted values is calculated at each time and fluence by

$$D_{\text{sq}}(H, t) = \frac{1}{N_\lambda} \sum_{j=1}^{N_\lambda} \left(\frac{Q(j, H, t)}{\max[|Q(j)|]} - \frac{Q'(j, H, t)}{\max[|Q'(j)|]} \right)^2, \quad (5)$$

with the number of discrete probe wavelengths N_λ , the measured quantity Q , and the fitted quantity Q' , both being representatives for the measured and fitted n , k , and R . The comparison of D_{sq} for the Drude and the Lorentz model, respectively, summarizes two main results (Fig. 4),

Firstly, the Lorentz as well as the Drude model reproduce the measured k and R quite well. However, the Drude model deviates much more from the measured n than the Lorentz model in the whole time-fluence parameter field, and, thus, the Drude model is not able to correctly describe the transient dielectric function of the excited fused silica. Instead, the transient optical properties during excitation are only reasonably

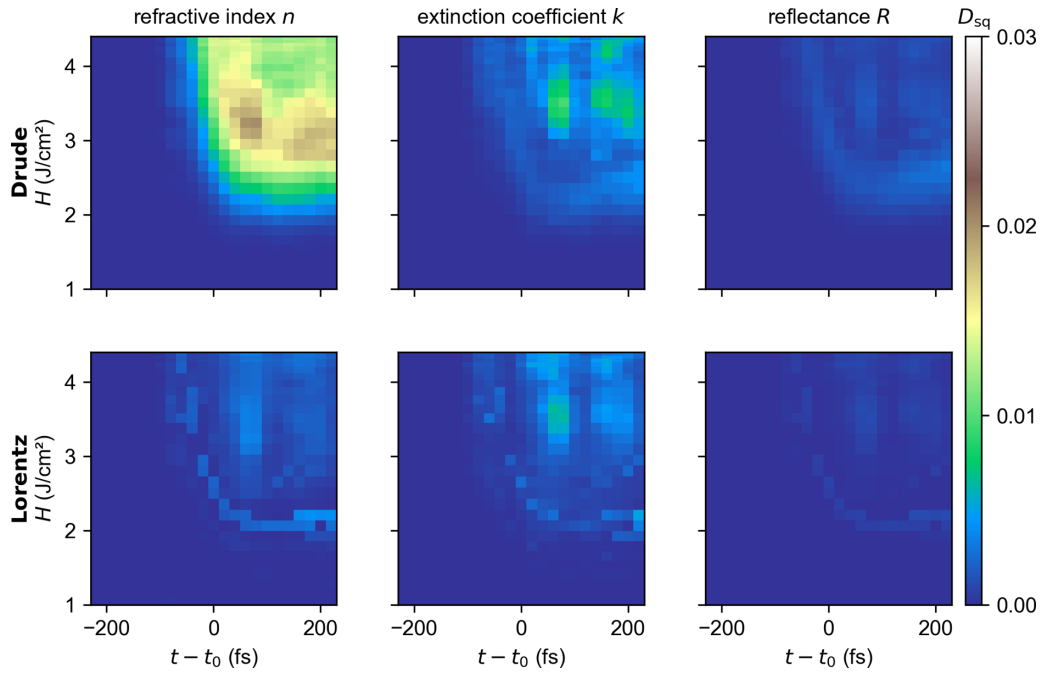


FIG. 4. Sum of the normalized squared residuals D_{sq} among n , k , and R measured by pump-probe ellipsometry and the approximated values by the Drude (top row) and the Lorentz model (bottom row) as a function of time as well as the fluence of the exciting pump radiation.

described by the Lorentz model. This means that, contrary to the state of the art, the excited electrons in amorphous fused silica cannot be simply considered as a nearly free-electron

plasma during the investigated temporal range up to 200 fs after irradiation. The electrons seem to be excited into bound-like states, probably due to a strong interaction of the electrons

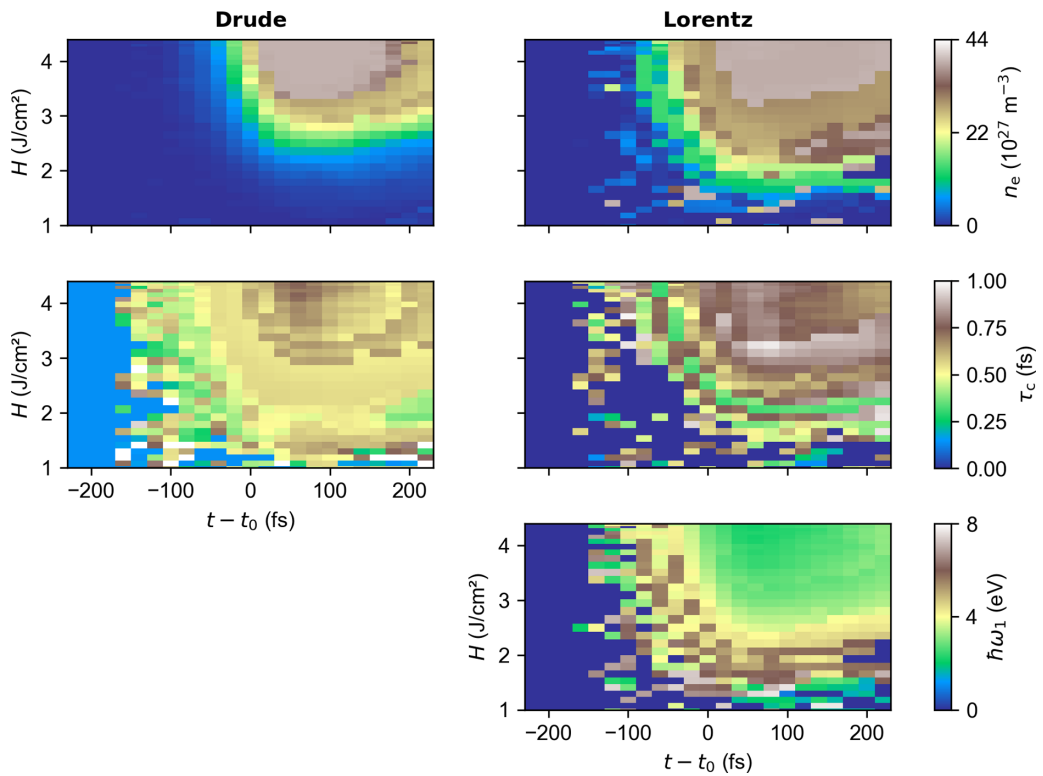


FIG. 5. Calculated spatially and temporally resolved electron density n_e , collision time τ_c , and resonance frequency energy $\hbar\omega_1$ of the electrons in the conduction band of fused silica induced by pump radiation with $H_0 = 4.4 \text{ J/cm}^2$ determined by the approximated Drude and Lorentz models from Eqs. (2) and (4).

with the surrounding disordered ions. However, this result does not exclude that the excited electrons will become nearly free at later times $t > 200$ fs due to a transition into the plasma state.

Second, the deviation D_{sq} of k and R approximated by the Drude model is much lower than for n and quite similar to the Lorentz model. This implies, that the approximation of the transient optical properties by a Drude model is quite reasonable when only the transient reflectance or absorbance is measured as was the state of the art until now. Since a lot of previous studies applied pump-probe reflectometry instead of pump-probe ellipsometry to investigate the nonlinear electron excitation in dielectrics, the Drude model seemingly represented a good first-order approximation to describe the transient optical properties in these studies [14,19,24,33,34,36,37,40,43,50,54].

Despite the differences in the resulting optical properties, the determined fitting parameters $n_e(t, H(x))$ and $\tau_c(t, H(x))$ are quite similar for both models (Fig. 5). Before irradiation at $t \ll t_0$, the electron density is approximately $n_e = 0$, and, thus, the Lorentz term describing the optical properties of fused silica at rest dominates in Eq. (2) as well as in Eq. (4). At $t > t_0$ and fluences $H > 3$ J/cm², the electron density reaches its constrained maximum of $n_e = 44 \times 10^{27}$ m⁻³ for both models. At $t < t_0$ and fluences $H < 2$ J/cm², the fitted collision times τ_c are quite noisy because $n_e = 0$ prevents an unambiguously determination of τ_c . After t_0 and at $H > 2$ J/cm², the Drude as well as the Lorentz models yield collision times in the range of 0.4 fs $< \tau_c < 0.8$ fs, being comparable to collision times in the range of 0.1 fs $< \tau_c < 2$ fs given in the literature [14,17,21,48]. The estimated resonance energy of the conduction-band electrons described by the Lorentz model is 2.5 eV $< \hbar\omega_1 < 4$ eV. This represents a reasonable range for $\hbar\omega_1$ since impact excitation requires the successive linear excitation of the electrons and transient transitions within the conduction band, respectively [14,17,19,53].

IV. CONCLUSION

Fused silica has been irradiated by ultrashort single-pulsed laser radiation ($\lambda_{\text{pump}} = 800$ nm, $\tau_{\text{H,pump}} = 40$ fs, and $H_0 =$

4.4 J/cm²) whereas the transient complex refractive index \tilde{n} has been detected by spectroscopic imaging pump-probe ellipsometry as a function of the wavelength of the probe radiation (450 nm $\leq \lambda \leq 900$ nm), the fluence of the pump radiation ($0 \leq H \leq 4.4$ J/cm²), and the temporal delay between pump and probe radiation (-200 fs $\leq (t - t_0) \leq 200$ fs). The transient refractive index $n(\lambda, H, t)$, the extinction coefficient $k(\lambda, H, t)$, as well as the reflectance $R(\lambda, H, t)$ were derived from the measured \tilde{n} . Two different dielectric function models were approximated to the measured transient optical properties. First, the state-of-the-art Drude model describes the excited electrons as nearly free. Second, the new approach based on a Lorentz model considers the excited electrons as bound. The applied Lorentz model replicates the measured refractive index n , the extinction coefficient k , and the reflectance R very well in the considered parameter range, whereas the Drude model only reproduces the reflectance and the extinction coefficient and strongly deviates from the measured transient refractive index. The deviation of the state-of-the-art Drude model from the measured transient optical properties implies that the excited electrons cannot be considered as a nearly free-electron plasma in the considered temporal range. Contrary, the significant lower deviation of the Lorentz model from the measured data indicates that the electrons are excited into bound states. These bound states might result from the interaction of the electrons with the surrounding disordered ions of the amorphous fused silica. In consequence, the established models for describing the dynamics of excited electrons, the transient optical properties, and the impact excitation rate based on free carrier absorption have to be reconsidered for fused silica.

ACKNOWLEDGMENTS

We gratefully thank the European Social Fund for Germany (ESF) for funding Project EilaSax (Project No. 100339506) and the Deutsche Forschungsgemeinschaft (DFG) by Contract No. INST 522/14-1 FUGG.

-
- [1] F. Kotz, P. Risch, K. Arnold, S. Sevim, J. Puigmartí-Luis, A. Quick, M. Thiel, A. Hrynevich, P. D. Dalton, D. Helmer, and B. E. Rapp, Fabrication of arbitrary three-dimensional suspended hollow microstructures in transparent fused silica glass, *Nat. Commun.* **10**, 1439 (2019).
 - [2] S. M. Eaton, C. de Marco, R. Martinez-Vazquez, R. Ramponi, S. Turri, G. Cerullo, and R. Osellame, Femtosecond laser microstructuring for polymeric lab-on-chips, *J. Biophoton.* **5**, 687 (2012).
 - [3] O. Tokel, A. Turnali, G. Makey, P. Elahi, T. Çolakoğlu, E. Ergeçen, Ö. Yavuz, R. Hübner, M. Z. Borra, I. Pavlov, A. Bek, R. Turan, D. K. Kesim, S. Tozburun, S. Ilday, and F. Ö. Ilday, In-chip microstructures and photonic devices fabricated by nonlinear laser lithography deep inside silicon, *Nat. Photonics* **11**, 639 (2017).
 - [4] T. Viertel, L. Pabst, M. Olbrich, R. Ebert, A. Horn, and H. Exner, Generation of nano-voids inside polylactide using femtosecond laser radiation, *Appl. Phys. A* **123**, 789 (2017).
 - [5] M. Kumagai, N. Uchiyama, E. Ohmura, R. Sugiura, K. Atsumi, and K. Fukumitsu, Advanced dicing technology for semiconductor wafer—stealth dicing, *IEEE Trans. Semicond. Manuf.* **20**, 259 (2007).
 - [6] H. Kämmer, G. Matthäus, S. Nolte, M. Chanal, O. Utéza, and D. Grojo, In-volume structuring of silicon using picosecond laser pulses, *Appl. Phys. A* **124**, 302 (2018).
 - [7] R. Le Harzic, R. Bückle, C. Wüllner, C. Donitzky, and K. König, Laser safety aspects for refractive eye surgery with femtosecond laser pulses, *Med. Laser Appl.* **20**, 233 (2005).

- [8] X. Yao, T. Ito, and D. A. Higgins, Grayscale patterning of polymer thin films with nanometer precision by direct-write multiphoton photolithography, *Langmuir* **24**, 8939 (2008).
- [9] L. Wang, X.-W. Cao, C. Lv, H. Xia, W.-J. Tian, Q.-D. Chen, S. Juodkazis, and H.-B. Sun, Formation of deep-subwavelength structures on organic materials by femtosecond laser ablation, *IEEE J. Quantum Electron.* **54**, 9200207 (2018).
- [10] B. Rethfeld, Unified Model for the Free-Electron Avalanche in Laser-Irradiated Dielectrics, *Phys. Rev. Lett.* **92**, 187401 (2004).
- [11] L. V. Keldysh, Ionization in the field of a strong electromagnetic wave, *JETP* **20**, 1307 (1965).
- [12] T. Pflug, P. Lungwitz, M. Olbrich, and A. Horn, Linear and nonlinear excitation of P3HT induced by spectral-shaped ultrafast mid-ir laser radiation, *J. Phys. Chem. C* **124**, 13618 (2020).
- [13] B. Chimier, O. Utéza, N. Sanner, M. Sentis, T. Itina, P. Lassonde, F. Légaré, F. Vidal, and J. C. Kieffer, Damage and ablation thresholds of fused-silica in femtosecond regime, *Phys. Rev. B* **84**, 094104 (2011).
- [14] M. Garcia-Lechuga, L. Haahr-Lillevang, J. Siegel, P. Balling, S. Guizard, and J. Solis, Simultaneous time-space resolved reflectivity and interferometric measurements of dielectrics excited with femtosecond laser pulses, *Phys. Rev. B* **95**, 214114 (2017).
- [15] T. Winkler, P. Balling, B. Zielinski, C. Sarpe, N. Jelzow, R. Ciobotea, A. Senftleben, and T. Baumert, Unveiling nonlinear regimes of light amplification in fused silica with femtosecond imaging spectroscopy, *Phys. Rev. Research* **2**, 023341 (2020).
- [16] B. C. Stuart, M. D. Feit, S. Herman, A. M. Rubenchik, B. W. Shore, and M. D. Perry, Nanosecond-to-femtosecond laser-induced breakdown in dielectrics, *Phys. Rev. B* **53**, 1749 (1996).
- [17] P. Balling and J. Schou, Femtosecond-laser ablation dynamics of dielectrics: Basics and applications for thin films, *Rep. Prog. Phys.* **76**, 036502 (2013).
- [18] L. V. Keldysh, Kinetic theory of impact ionization in semiconductors, *JETP* **10**, 509 (1960).
- [19] K. Wædegaard, M. Frislev, and P. Balling, Femtosecond laser excitation of dielectric materials: Experiments and modeling of optical properties and ablation depths, *Appl. Phys. A* **110**, 601 (2013).
- [20] Arnold and Cartier, Theory of laser-induced free-electron heating and impact ionization in wide-band-gap solids, *Phys. Rev. B* **46**, 15102 (1992).
- [21] Arnold, Cartier, and DiMaria, Acoustic-phonon runaway and impact ionization by hot electrons in silicon dioxide, *Phys. Rev. B* **45**, 1477 (1992).
- [22] A. Kaiser, B. Rethfeld, M. Vicanek, and G. Simon, Microscopic processes in dielectrics under irradiation by subpicosecond laser pulses, *Phys. Rev. B* **61**, 11437 (2000).
- [23] D. Du, X. Liu, G. Korn, J. Squier, and G. Mourou, Laser-induced breakdown by impact ionization in sio 2 with pulse widths from 7 ns to 150 fs, *Solid-State Electron.* **64**, 3071 (1994).
- [24] D. von der Linde and H. Schüler, Breakdown threshold and plasma formation in femtosecond laser–solid interaction, *J. Opt. Soc. Am. B* **13**, 216 (1996).
- [25] L. Hallo, A. Bourgeade, V. T. Tikhonchuk, C. Mezel, and J. Breil, Model and numerical simulations of the propagation and absorption of a short laser pulse in a transparent dielectric material: Blast-wave launch and cavity formation, *Phys. Rev. B* **76**, 024101 (2007).
- [26] X.-X. Liang, Z. Zhang, and A. Vogel, Multi-rate-equation modeling of the energy spectrum of laser-induced conduction band electrons in water, *Opt. Express* **27**, 4672 (2019).
- [27] N. Linz, S. Freidank, X.-X. Liang, and A. Vogel, Wavelength dependence of femtosecond laser-induced breakdown in water and implications for laser surgery, *Phys. Rev. B* **94**, 024113 (2016).
- [28] M. Li, S. Menon, J. P. Nibarger, and G. N. Gibson, Ultrafast Electron Dynamics in Femtosecond Optical Breakdown of Dielectrics, *Phys. Rev. Lett.* **82**, 2394 (1999).
- [29] P. K. Kennedy, A first-order model for computation of laser-induced breakdown thresholds in ocular and aqueous media. i. theory, *IEEE J. Quantum Electron.* **31**, 2241 (1995).
- [30] P. K. Kennedy, S. A. Boppart, D. X. Hammer, B. A. Rockwell, G. D. Noojin, and W. P. Roach, A first-order model for computation of laser-induced breakdown thresholds in ocular and aqueous media. ii. comparison to experiment, *IEEE J. Quantum Electron.* **31**, 2250 (1995).
- [31] T. Pflug, M. Olbrich, and A. Horn, Surface modifications of poly(methyl methacrylate) induced by controlled electronic and molecular vibrational excitation applying ultrafast mid-ir laser radiation, *J. Phys. Chem. C* **123**, 20210 (2019).
- [32] P. P. Rajeev, M. Gertsvolf, P. B. Corkum, and D. M. Rayner, Field Dependent Avalanche Ionization Rates in Dielectrics, *Phys. Rev. Lett.* **102**, 083001 (2009).
- [33] D. Satoh, T. Shibuya, E. Terasawa, Y. Moriai, H. Ogawa, M. Tanaka, Y. Kobayashi, and R. Kuroda, Ultrafast pump-probe microscopic imaging of femtosecond laser-induced melting and ablation in single-crystalline silicon carbide, *Appl. Phys. A* **126**, 795 (2020).
- [34] D. Puerto, W. Gawelda, J. Siegel, J. Bonse, G. Bachelier, and J. Solis, Transient reflectivity and transmission changes during plasma formation and ablation in fused silica induced by femtosecond laser pulses, *Appl. Phys. A* **92**, 803 (2008).
- [35] L. Haahr-Lillevang, K. Wædegaard, D. B. Sandkamm, A. Mouskeftaras, S. Guizard, and P. Balling, Short-pulse laser excitation of quartz: Experiments and modelling of transient optical properties and ablation, *Appl. Phys. A* **120**, 1221 (2015).
- [36] D. Puerto, J. Siegel, W. Gawelda, M. Galvan-Sosa, L. Ehrentraut, J. Bonse, and J. Solis, Dynamics of plasma formation, relaxation, and topography modification induced by femtosecond laser pulses in crystalline and amorphous dielectrics, *J. Opt. Soc. Am. B* **27**, 1065 (2010).
- [37] A. Q. Wu, I. H. Chowdhury, and X. Xu, Femtosecond laser absorption in fused silica: Numerical and experimental investigation, *Phys. Rev. B* **72**, 085128 (2005).
- [38] L. Jiang and H.-L. Tsai, A plasma model combined with an improved two-temperature equation for ultrafast laser ablation of dielectrics, *J. Appl. Phys.* **104**, 093101 (2008).
- [39] J. Hernandez-Rueda, J. J. Witcher, and D. M. Krol, Ultrafast time-resolved spectroscopy of a fs-laser-induced plasma inside glass using a super-continuum probe beam, *Appl. Phys. A* **125**, 591 (2019).
- [40] M. Lebugle, N. Sanner, N. Varkentina, M. Sentis, and O. Utéza, Dynamics of femtosecond laser absorption of fused silica in the ablation regime, *J. Appl. Phys.* **116**, 063105 (2014).
- [41] M. H. Mahdieh, M. A. Jafarabadi, and D. Katozzi, Time-resolved optical probing of nanosecond laser-induced break-

- down plasma in polymethyl methacrylate (pmma), *Appl. Phys. B* **124**, 26 (2018).
- [42] N. M. Bulgakova, V. P. Zhukov, S. V. Sonina, and Y. P. Meshcheryakov, Modification of transparent materials with ultrashort laser pulses: What is energetically and mechanically meaningful?, *J. Appl. Phys.* **118**, 233108 (2015).
- [43] I. H. Chowdhury, A. Q. Wu, X. Xu, and A. M. Weiner, Ultrafast laser absorption and ablation dynamics in wide-band-gap dielectrics, *Appl. Phys. A* **81**, 1627 (2005).
- [44] S. Guizard, P. Martin, G. Petite, P. D'Oliveira, and P. Meynadier, Time-resolved study of laser-induced colour centres in, *J. Phys.: Condens. Matter* **8**, 1281 (1996).
- [45] P. Martin, S. Guizard, P. Daguzan, G. Petite, P. D'Oliveira, P. Meynadier, and M. Perdrix, Subpicosecond study of carrier trapping dynamics in wide-band-gap crystals, *Phys. Rev. B* **55**, 5799 (1997).
- [46] F. Quéré, S. Guizard, and P. Martin, Time-resolved study of laser-induced breakdown in dielectrics, *Europhys. Lett.* **56**, 138 (2001).
- [47] T. Pflug, M. Olbrich, R. Roesch, U. S. Schubert, H. Hoppe, and A. Horn, Investigations on the modification of pmma by ultrafast laser radiation from the uv to the mid-ir spectral range, *Opt. Lasers Eng.* **111**, 130 (2018).
- [48] G. C. Nagar, D. Dempsey, and B. Shim, Wavelength scaling of electron collision time in plasma for strong field laser-matter interactions in solids, *Commun. Phys.* **4**, 96 (2021).
- [49] P. Jürgens, M. J. J. Vrakking, A. Husakou, R. Stoian, and A. Mermillod-Blondin, Plasma formation and relaxation dynamics in fused silica driven by femtosecond short-wavelength infrared laser pulses, *Appl. Phys. Lett.* **115**, 191903 (2019).
- [50] K. Sokolowski-Tinten and D. von der Linde, Generation of dense electron-hole plasmas in silicon, *Phys. Rev. B* **61**, 2643 (2000).
- [51] V. V. Temnov, K. Sokolowski-Tinten, P. Zhou, A. El-Khamhawy, and D. von der Linde, Multiphoton Ionization in Dielectrics: Comparison of Circular and Linear Polarization, *Phys. Rev. Lett.* **97**, 237403 (2006).
- [52] S. S. Mao, F. Qur, S. Guizard, X. Mao, R. E. Russo, G. Petite, and P. Martin, Dynamics of femtosecond laser interactions with dielectrics, *Appl. Phys. A* **79**, 1695 (2004).
- [53] B. H. Christensen and P. Balling, Modeling ultrashort-pulse laser ablation of dielectric materials, *Phys. Rev. B* **79**, 155424 (2009).
- [54] B. Davidson, G. Lucovsky, G. Parsons, R. Nemanich, A. Esser, K. Seibert, and H. Kurz, Free carrier absorption and the transient optical properties of amorphous silicon thin films: A model including time dependent free carrier, and static and dispersive interband contributions to the complex dielectric constant, *J. Non-Cryst. Solids* **114**, 579 (1989).
- [55] H. Wang and H. Shen, A prediction model for ablation fluence threshold in femtosecond laser processing of fused silica, *J. Micro Nano-Manuf.* **5**, 031006 (2017).
- [56] S. Guizard, A. Semerok, J. Gaudin, M. Hashida, P. Martin, and F. Quéré, Femtosecond laser ablation of transparent dielectrics: measurement and modelisation of crater profiles, *Appl. Surf. Sci.* **186**, 364 (2002).
- [57] V. Recoules, J. Clérouin, G. Zérah, P. M. Anglade, and S. Mazevet, Effect of Intense Laser Irradiation On the Lattice Stability of Semiconductors and Metals, *Phys. Rev. Lett.* **96**, 055503 (2006).
- [58] C. F. Klingshirn, *Semiconductor Optics* (Springer, Berlin/Heidelberg, 2012)
- [59] M. Gertsvolf, M. Spanner, D. M. Rayner, and P. B. Corkum, Demonstration of attosecond ionization dynamics inside transparent solids, *J. Heat Transfer* **43**, 131002 (2010).
- [60] I. H. Malitson, Interspecimen comparison of the refractive index of fused silica, *J. Opt. Soc. Am.* **55**, 1205 (1965).
- [61] R. Kitamura, L. Pilon, and M. Jonasz, Optical constants of silica glass from extreme ultraviolet to far infrared at near room temperature, *Appl. Opt.* **46**, 8118 (2007).
- [62] See Supplemental Material at <http://link.aps.org/supplemental/10.1103/PhysRevB.106.014307> for a detailed explanation of the ellipsometric principle, the experimental setup, the evaluation methods, and the whole measured data set.
- [63] T. Q. Jia, Z. Z. Xu, R. X. Li, D. H. Feng, X. X. Li, C. F. Cheng, H. Y. Sun, N. S. Xu, and H. Z. Wang, Mechanisms in fs-laser ablation in fused silica, *J. Appl. Phys.* **95**, 5166 (2004).
- [64] H. Fujiwara, *Spectroscopic Ellipsometry: Principles and Applications* (Wiley, Chichester/Hoboken, 2009).
- [65] T. Pflug, J. Wang, M. Olbrich, M. Frank, and A. Horn, Case study on the dynamics of ultrafast laser heating and ablation of gold thin films by ultrafast pump-probe reflectometry and ellipsometry, *Appl. Phys. A* **124**, 17572 (2018).
- [66] T. T. Winkler, *Laser Amplification in Excited Dielectrics* (Universitätsbibliothek Kassel, Kassel, 2018).